Multi-joint rigidity-testing device for titrating medication and deep brain stimulation therapies

A THESIS
SUBMITTED TO THE FACULTY OF THE GRADUATE SCHOOL
OF THE UNIVERSITY OF MINNESOTA
BY

Kevin J. Mohsenian

IN PARTIAL FULFILLMENT OF THE REQUIREMENTS
FOR THE DEGREE OF
MASTER OF SCIENCE

Dr. Matthew D. Johnson

August 2014

August 2014

Acknowledgements

I would like to thank my adviser, Dr. Matthew Johnson of the Biomedical Engineering Department. His guidance and support have been imperative in this research as well as in my development as a biomedical engineer. Additionally, I would like to acknowledge Allison Connolly, a graduate student in the Biomedical Engineering Department, and Dr. Abirami Muralidharan, a post-doc in the Department of Neurology. Allison and Abirami were integrally involved in the testing of the devices, participating as experimenters and providing feedback on the device designs. I also acknowledge the support of Dr. Filippo Agnesi, a post-doc in the Biomedical Engineering Department who contributed feedback and technical assistance during the study. In addition, David Moreno, an undergraduate in the Biomedical Engineering department, contributed to the initial testing of sensors and data acquisition set-up, and I appreciate his contribution. Also, I thank the University of Minnesota Design of Medical Device Center for providing the prototyping resources needed in this study.

Furthermore, I would like to thank Dr. Hubert Lim of the Biomedical Engineering Department and Dr. Ken Baker of the Department of Neurology for both supporting my education as well as my research and also for serving as members of my committee. Finally, I would like to thank fellow lab members Laura Zitella, Ben Teplitzky, and Joe Xiao for their support and technical assistance.

Abstract

Disabling motor signs of Parkinson's Disease including akinesia, bradykinesia, tremor, and muscle rigidity are typically quantified by clinicians using the Unified Parkinson's Disease Rating Scale (UPDRS). These subjective assessments, while useful, often vary among clinicians, making it challenging to evaluate medication and deep brain stimulation (DBS) therapies in multi-center trials. In this study, two designs for a multi-joint rigidity-testing device were developed to enable objective, quantitative measures of rigidity. The investigator passively manipulated the subject's joints while stabilizing the appendage distal to the joint with two opposing force transducers, providing a measurement of differential force during the movement. These forces were synchronized to the joint angle, measured by a motion capture camera system. Here, we show feasibility data for detecting changes in muscle rigidity in a parkinsonian non-human primate treated with Sinemet, Globus Pallidus internal (GPi) DBS and/or subthalamic nucleus (STN) DBS.

For design 1, the device was tested on six joints: elbow, wrist, shoulder, hip, knee and ankle, and in three states: MPTP, DBS stimulation, and drug therapy. Device 1 was effectively able to quantify rigidity and determine changes in rigidity states among all joints except elbow ($p<0.05$). For design 2, the device was tested on only the shoulder abduction/adduction and was tested in three states: MPTP, DBS stimulation, and post-DBS stimulation. Design 2 was effectively able to quantify changes in rigidity as well ($p<0.05$). Ergonomics and durability were considered in the evaluation of the devices. While each device showed promising results, future iterations will also need to address several limitations of the current devices. The eventual goal of this rigidity testing device would be to use it in the clinic to assist neurologists in titrating medication levels and DBS parameters.

Table of Contents

Table of Contents (continued)

List of Tables

List of Figures

Introduction

Parkinson's Disease (PD), as with many other neurodegenerative brain disorders, is becoming more prevalent as the population ages. An estimated five million people worldwide live with PD and the prevalence is expected to increase exponentially in the coming years (Xia et. al. 2012). The current prevalence is approximately 0.3% for the overall populations of industrialized countries and 1% for the populations over 60 years old (de Lau et. al. 2004). When a patient is diagnosed with PD, this indicates the degeneration of the dopaminergic neurons in the brain, depleting especially in the substantia nigra pars compacta (SNc), which is the main source of dopamine in the brain (Galvan and Wichmann 2008). The SNc is part of the basal ganglia (BG) which also includes the striatum, nucleus accumbens, Globus Pallidus (GP), and Subthalamic Nucleus (STN). When the SNc no longer transmits DA to the other BG nuclei, neural pathways begin to disassemble and degeneration to these nuclei begins. This degeneration causes the neural circuits to fall out of balance which affects downstream structures, such as the motor cortex (Mazzoni 2012).

Currently, there is no cure for PD, but there are several therapies available to patients when symptoms impair normal motor control. Dopamine replacement therapy using Levodopa (L-dopa; 3,4-dihydroxyphenyl-L-alanine), or another dopamine agonist, is the initial therapy used with PD patients (Xia et. al. 2012). While L-dopa remains the gold standard, drug-induced motor symptoms, such as dyskinesia, decrease the quality of life for PD patients (Schrag et. al. 2000). Additionally, L-dopa does not prevent the degeneration from the disease (Xia et. al. 2012). For some patients, the progression of the disease has caused them to become resistant to the drug therapy, or drug-intractable. It is hypothesized that the loss of dopaminoreceptive neurons in diseased patients causes L-dopa resistance (Chiba et. al. 2012). For drug-intractable patients, more options are available but there are increased risks and costs. Deep brain stimulation (DBS) and neuroprotective drug therapies are currently being investigated (Johnson et. al. 2008, Xia et. al. 2012).

PD is a neurodegenerative brain disorder that results in a broad range of disabling motor signs, including akinesia, bradykinesia, tremor, and muscle rigidity (Mazzoni

2012). Rigidity, one of the cardinal symptoms of PD, can be equated to the amount of resistance to passively move a limb (Mazzoni 2012), independent of velocity and direction (Delwaide 2001). This is a common symptom that makes a patient stiff and can be easily evaluated during a patient's visit to the physician. It is proposed that the increase in muscle stiffness observed through passive manipulation (Fung et al. 2000, Rätsep and Asser 2011) is due to the increase in the long-latency stretch reflex (Berardelli et al. 1983, Meara and Cody 1993) of the muscle (Xia et. al. 2012).

To determine the progression of a patient's PD, a physician will use the Unified Parkinson's Disease Rating Scale (UPDRS, section III) which quantifies the severity of motor signs from 0 (normal) to 4 (severe). These subjective assessments, while useful, often vary among clinicians (Imbert et. al. 2000, Patrick et. al. 2001), making it challenging to evaluate medication and deep brain stimulation (DBS) therapies in multi-center trials (Van Dillon et. al. 1988). While using this scale is relatively accurate, there are disparities between physicians and between visits. Having a way to quantify these movements and rigidity would be ideal to give proper help to patients.

One way to determine the success of a therapy is to quantify the changes in a patient's symptoms in response to the therapy. Due to the controllable, passive method of assessing rigidity, quantifying rigidity has become a common method for determining therapeutic improvement. Additionally, parkinsonian rigidity has shown to track the progression of the disease in comparison to the other cardinal symptoms (Louis et. al. 1999). Futhermore, rigidity seems to react well with drug treatment (Vu et. al. 2012) which is important for evaluating pharmaceutical therapies. Several previous studies have developed biomechanical devices to measure muscle rigidity at different joints in both human and non-human primates (NHPs) (See Table 1). Many attempts have used motorized actuators that can be selectively programmed to articulate joints across a range of angles and frequencies. However, correlating the results from these studies with clinical assessments of rigidity prove inconsistent (Prochazka et. al. 1997). While these devices have shown the feasibility to measure force changes at a specific joint, most devices are not usable with other joints, limiting their clinical use. In most cases, not all joints receive the same amount of improvement from a therapy; therefore, a single joint approach could be flawed. Emerging therapy testing is conducted in NHPs as the

parkinsonian NHP model has shown to be very effective at portraying PD motor symptoms (Fox 2010). Therefore, developing a device for NHPs to quantify the benefits of novel therapeutic techniques is in high demand.

Table 1: Previous Research Quantifying Rigidity in PD

Reference	Rigidity sensor(s)	Angle/Position tracking	Joint of interest
Webster, 1959*	load cell	Turntable (fixed movements)	Elbow
Kondraske, 1984*	strain gauge	potentiometer	Elbow, Knee
Lakie, 1984*	suction EMG electrodes	potentiometer	Wrist
Watts, 1986*	strain gauge	magnetoresistive potentiometer	Elbow
Chan, 1987*	force transducer	potentiometer	Knee
Brown, 1988	angular velocity profile	goniometer	Knee
Caligiuri, 1989*	resistive strain gauges	potentiometer	Finger
Caligiuri, 1992*	force transducer	rotation transducer	Finger
Caligiuri, 1994	resistive strain gauges	linear potentiometer	Wrist
Relja, 1996	torque sensor	potentiometer	Elbow
Prochazka, 1997	two air-filled force pads	length gauge	Elbow
Fung, 2000*	torque motor output	potentiometer	Wrist
Patrick, 2001	air-filled differential force transducer	Piezoelectric gyroscope	Wrist, Elbow
Xia, 2004*	surface EMG electrodes	motor axis rotation	Wrist
Shapiro, 2007*	torque transducer	capacitative transducer	Elbow
Hong, 2007	*Rigidity analyzer*®	solid-state gyroscope	Elbow
Mak, 2007*	dynamometer	motor axis rotation	Trunk
Sepehri, 2007	strain gauge transducer	potentiometer	Elbow
Endo, 2009	three-axis force sensors	gyroscope	Elbow
Levin, 2009	Ag-Cl surface EMG electrodes	goniometer	Elbow
Mera, 2009*^	three-axis force transducer	motor axis rotation	Elbow
Cano-de-la-Cuerda, 2011	dynamometer	motor axis rotation	Trunk
Niazmond, 2011	sheet force sensor	3-axis acceleration sensors	Elbow
Park, 2011	load cell	potentiometer	Wrist
Little, 2012	strain gauge	goniometer	Wrist
Dai, 2013	force sensitive resistors	3-axis gyroscope	Elbow

* - indicates device is actuated ^ - indicates primate study

Rigidity analyzer® is developed by Neurokinetics (Edmonton, AB).

In this study, we developed a multi-joint rigidity-testing device to enable objective, quantitative measures of rigidity with millisecond resolution. The investigator

passively manipulated the subject's joints while stabilizing the appendage distal to the joint with two opposing force transducers, providing a measurement of differential force during the movement. These forces were synchronized to the joint angle, measured by a motion capture camera system. Here, we show the development, calibration, and validation of a multi-joint device for detecting changes in muscle rigidity in parkinsonian NHPs treated with Sinemet, GPi-DBS and/or STN-DBS.

Materials and Methods

Non-human primate subjects

This study involved rigidity testing, performed on two rhesus monkeys (*Macacca mulatta*) that were previously rendered parkinsonian. Subject P (19 y.o., ♀, 10.0 kg) was systemically induced parkinsonian with 3 daily injections of 1-methyl-4-phenyl-1,2,3,6-tetrahydropyridine (MPTP, Toronto Research Chemicals Inc., Brisbane, Ontario, 0.4-0.6 mg/kg) causing severe parkinsonian symptoms, and had two DBS leads implanted in the STN and GPi. In contrast, Subject F (18 y.o., ♀, 10.2 kg) was given several inter-carotid injections of MPTP which produced mild symptoms and had one DBS lead implanted in the STN. These subjects tested out two different device designs. All procedures were approved by the Institutional Animal Care and Use Committee of the University of Minnesota and complied with United States Public Health Service policy on the humane care and use of laboratory animals.

Force Sensor and DAQ Selection

Based on previous research shown in Table 1, there are several force sensors that could be used, such as load cells, strain gauges, force sensitive resistors (FSRs), and many other torque sensors. An extensive search was conducted on possible candidates for the device in this study (Table 2).

Table 2 – Force sensor comparison

Name	Company	Type	Height	Force Range	Cost per sensor
Flexiforce	Tekscan	Force Sensitive Resistor	1 mm	circuit dependent	$25
FC2231	Measurement Specialties	Load Cell	25 mm	0 to 100 lbf	$45
KDN 1865	Honeywell	Force transducer	7.62 mm	0 to 50 lbf	$102
FS03	Honeywell	Force transducer	16 mm	0 to 3 lbf	$115
Mini-45	ATI	Force transducer	15.7 mm	0 to 120 lbf	$3,900*
Nano-25	ATI	Force transducer	21.6 mm	0 to 100 lbf	$4,250*

*Need to purchase interface board and cable which is an additional $1,885.

To determine the feasibility of using sensors that would not restrict the sensing on the limbs, hand measurements were taken to test the ergonomics of using a sensor with different heights. The set-up and results of this testing are shown in Appendix 1. Based on this analysis, all of the sensors above were determined to be feasible in terms of hand ergonomics, but the smaller the sensor height the better. The three sensors that were heavily considered were the Flexiforce FSRs, Measurement Specialties FC2231 load cells and ATI Nano-25 sensors. One of the main motivations for this project was to create a device that could be replicated by other labs and used to capture rigidity. The main goals for this study were to create a rigidity measuring device that is efficient, easy-to-use, and cost efficient. Therefore, FSRs were investigated first to see if they could be used to capture rigidity. Unfortunately, they were unable to be used due to the fact that the baseline for the sensors changed when the sensors were moved, meaning that the calculations for force changes could not be calculated (data not shown). The next sensor investigated was the FC 2231 load cell from Measurement specialties. After initial testing

of the sensors, it was determined that the FC 2231 sensors had the sensitivity to be used in our device.

For the data acquisition (DAQ) board selection, the two main DAQ systems considered were National Instruments DAQ (NI-DAQ) and Arduino. Since both the NI-DAQ and Arduino can be paired with Matlab, and additionally an Arduino is much more affordable, Arduino was initially chosen for testing of Device 1. The reason for pairing the data acquisition with Matlab is to streamline offline analysis, as well as develop a graphic user interface (GUI) in Matlab to provide feedback for the experimenter as a future direction.

Design of Device 1

The rigidity measuring device (Device 1) was composed of two FC 2231 load cells (Measurement Specialties, Hampton, VA) attached to the researcher's thumb and index/middle finger with Velcro straps (Velcro, Manchester, NH) (Figure 1B). Two metal stabilization plates were secured to opposite sides of the primate's limb with an adjustable Velcro strap. Indentations in the plates provided a stable point for pressure application of the load cells and minimized forces and torques in unwanted directions (Figure 1A). The Velcro attachments allow the rigidity-testing device to fit any size limb in order to test a variety of joints. The data from the sensors was transmitted to an Arduino Uno microcontroller (Ivrea, Italy). Position data was collected using an infrared motion capture system (Vicon, Centennial, CO) as shown in Figure 2A. Reflective markers were placed at strategic locations on the body of the non-human primate as well as on the researcher's hand. An analog synchronization output from the Vicon system was sent to the Arduino microcontroller to co-register the force and position data offline (Figure 2C).

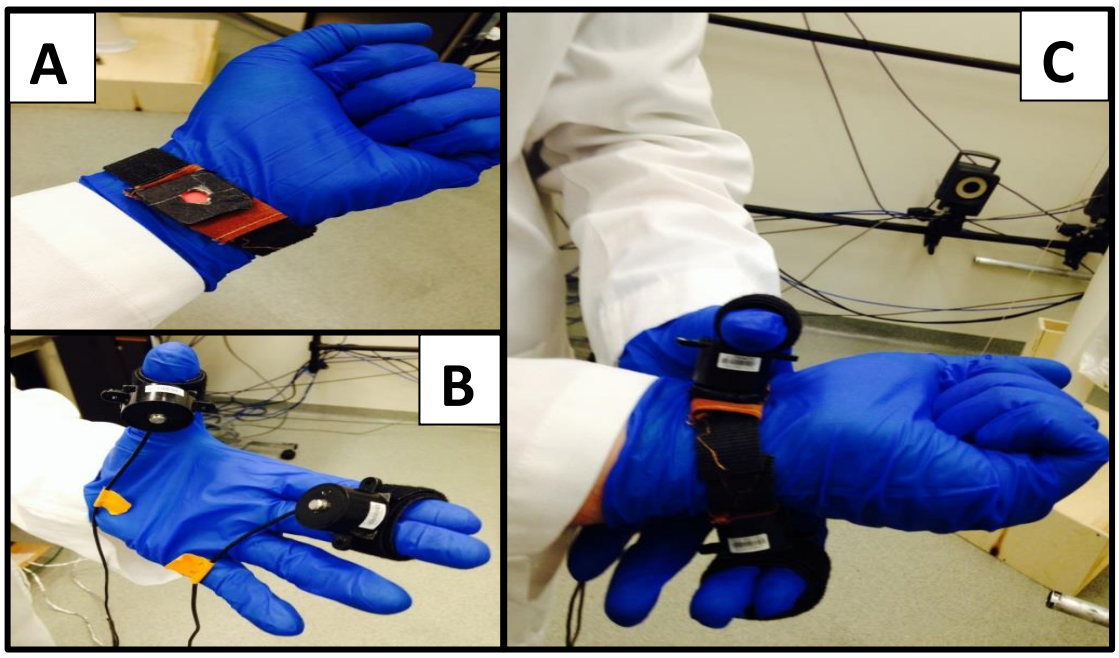

Figure 1: Device 1 sensor-transducer interface. A) For each transducer, a metal pad was sewn onto a brown fabric loop that slides along the Velcro to create a stable surface for each finger digit while minimizing torque on the transducer. With the transducers attached to the fabric loop, the set-up can be adjusted to different locations on the body to capture rigidity across multiple joints. B) Load cells were attached to digits 1 and 2/3 with Velcro. C) Shows the overall set-up for Device 1.

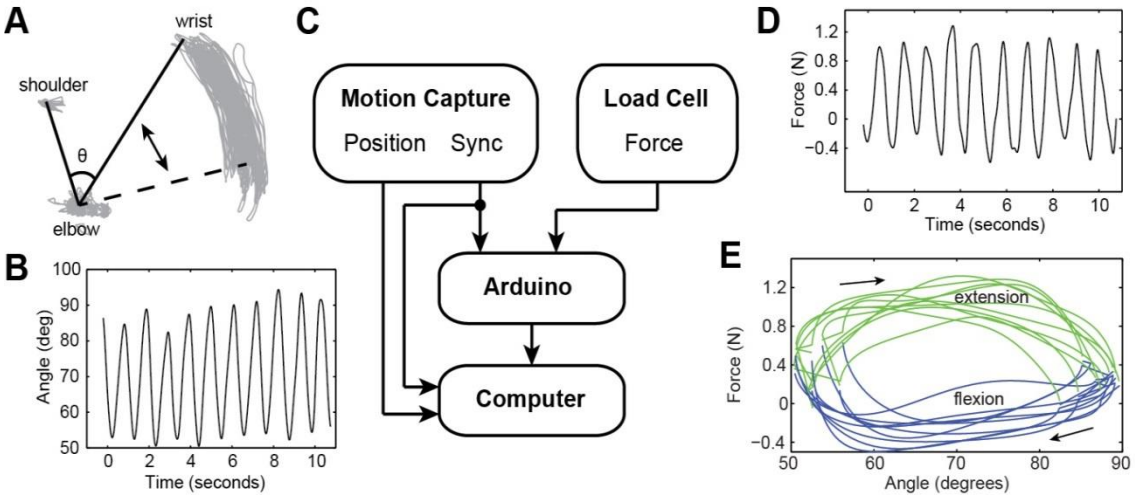

Figure 2: Device 1 schematic. A) Position of the shoulder, elbow, and wrist during elbow joint articulation. B) Elbow angle during articulations. C) Schematic drawing of data acquisition set-up for Device 1. D) Differential force measurements during elbow articulations. E) Force - angle curves of elbow flexion/extension.

While measuring rigidity is the same concept between humans and NHPs, through passive manipulation of the joints, cooperation to wear rigidity devices poses a limitation to most of the devices listed in Table 1. Therefore, one of the design elements of Device 1 was the experimenter's ability to release the limb of the animal if the animal was not allowing for passive manipulation. The device was designed so that the experimenter could easily detach the sensors and remove their hand from the animal. The Velcro strap used can adjust to the animal's limb, whether they were testing on the arm, leg, etc.

Design of Device 2

The second design for the rigidity measuring device is very similar to Device 1, since it is composed of two FC 2231 load cells (Measurement Specialities, Hampton, VA) but the sensors are connected with Velcro (Velcro, Manchester, NH) onto the limb of the animal and a 3D printed (acrylonitrile butadiene styrene) cap has been to fit onto the sensing tip of each sensor. This provides a surface for the thumb and fingers of the experimenter to rest and the height of the caps were designed so as to not touch the non-sensing areas of the sensors. This cap design should allow any pressure applied to the cap to be transferred to the sensor tip. Again, the Velcro attachments allow the rigidity-testing device to fit any size limb in order to test a variety of joints. For this second device the NI-DAQ (NI USB-6216) was used to acquire the data, since the infrared camera system was Motion Analysis (Santa Rosa, California) and the NI-DAQ feeds directly into the software interface of the Motion Analysis program. Unlike device 1, the force data is synced directly with the angle data in the Motion Analysis, so there is no need for a sync pulse and co-registration calculation.

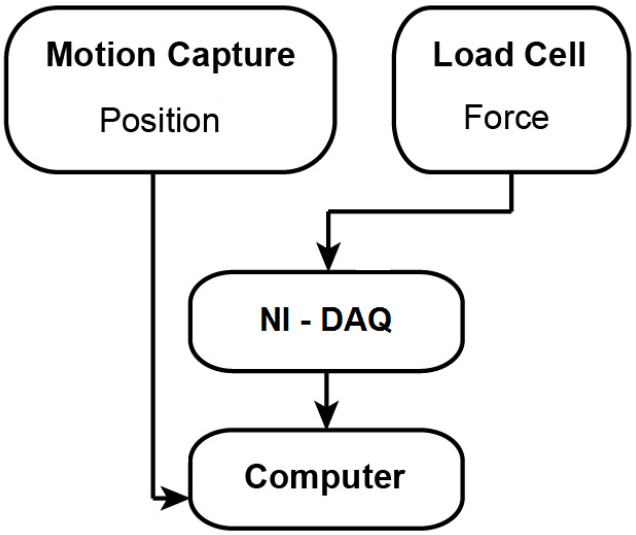

Figure 3: Device 2 schematic. Schematic drawing of data acquisition set-up for Device 2.

Reflective markers were placed at strategic locations on the body of the NHP as well as on the researcher's hand.

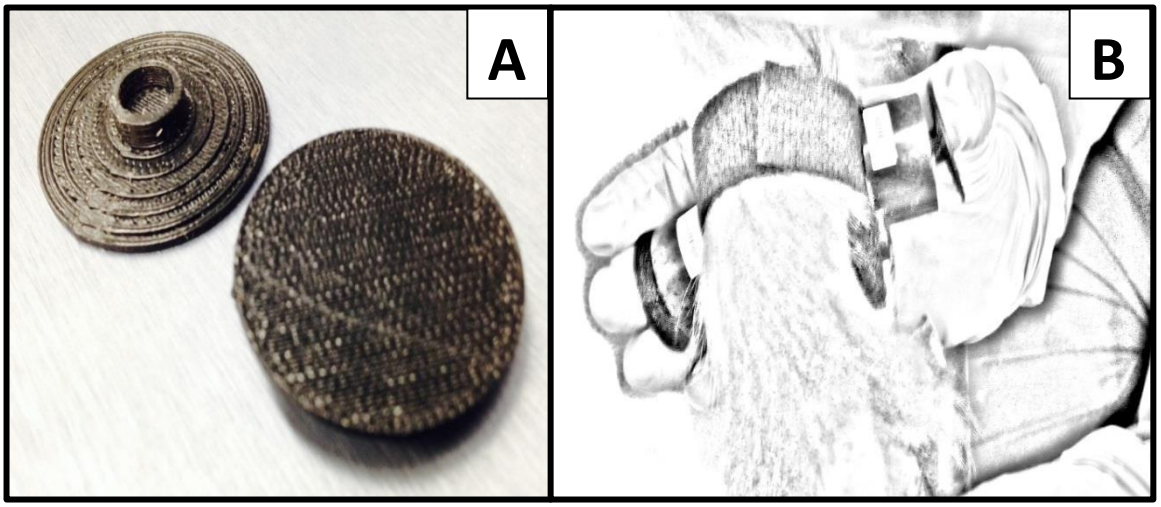

Figure 4: Device 2 cap–sensor interface. A) Two 3D printed caps used for Device 2. B) Device 2 set-up with the sensors velcroed to the forearm to manipulate the shoulder abduction/adduction, fingers rest on the caps of the device for rigidity measurement.

Calibration

Load Cell Calibration

A calibration device was built to translate voltage output from the load cells to actual force applied (see Figure 4). The sensors were each calibrated separately with known weights that were stacked onto the calibration device (Figure 4B). A small rectangular wooden box with open ends was built to stabilize the weighted end on the device. Zinc discs were tapped together into six bundles with five discs per bundle. Each bundle was labeled and measured on a digital scale prior to calibration testing. The Arduino and the NI-DAQ had different input currents so both microcontroller set-ups were calibrated.

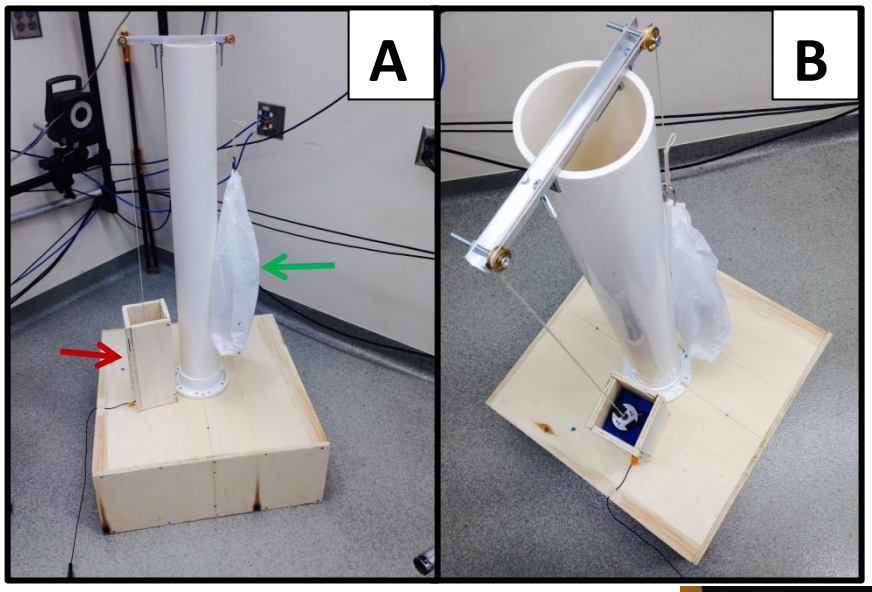

Figure 5: Calibration device. A) The calibration device has a weight-application rod that is hidden by the rectangular box (red arrow) which concentrates the weight onto of the load cell. The bag (green arrow) holds the counter-weight for the weight-application rod. B) The zinc discs are visible within the rectangular box.

Load Cell Sensitivity testing

After sensors were calibrated, the load cell sensitivity was investigated. To test how sensitive the load cells were to changes in resistance, a wooden 'arm' was built to be able to simulate movements with the differential sensor set-up. In addition, hooks were screwed in to be able to place rubber bands on the arm and add resistance. Unfortunately the data was inconclusive due to non-linearities in the rubber bands for the consistency in testing (data not shown).

Figure 6: Wooden Arm Calibration. Wooden arm has a rubber band hooked, acting as the bicep. Additionally three markers helped to calculate angle of the wooden elbow joint.

Load Cell Performance

Before conducting a study with parkinsonian NHPs, the sensors were tested on a human elbow to ensure the sensor differential set-up would capture changes in rigidity. To test the performance of the sensors, the sensors were tapped onto a healthy human forearm. The subject was asked to relax his elbow and allow passive manipulation. After several trials of passive movement, the subject was asked to resist movements to his elbow. The two

states can be compared to see if the overall concept for the device will be able to perform accurately.

Experimental Recordings

For the NHP experiments, both subjects were seated and awake. The NHPs were trained to allow passive joint manipulations months leading up to the device testing. For each trial, the animal was manipulated approximately 30 cycles (e.g. extension/flexion, abduction/adduction). Additionally, the experimenters were trained on how to properly use the rigidity measuring device prior to the experiments. With the relatively simple set-up of the device for experimenter convenience, the device-use training was a brief meeting prior to recording.

Subject P experiment

The stimulation settings for each animal were slightly different depending on the other protocols that were being investigated. The experimental procedure for Subject P helped to compare the effectiveness of therapies for PD as rigidity was tested under three experimental conditions: 1) MPTP, 2) MPTP+DBS, and 3) MPTP+Sinemet. The two DBS settings tested were the STN-DBS stimulation using 3 radial contacts each at 400 μA and at 130 Hz and GPi-DBS stimulation using 3 radial contacts each at 300 μA and at 130 Hz. For rigidity measuring during DBS therapy, stimulation was turned on for at least five minutes prior to performing passive manipulations.

After stimulation was terminated and given a >60 minute washout period, Sinemet therapy was given through oral administration of 200 mg (150 mg levodopa, 50 mg carbidopa, Merck, Whitehouse Station, NJ). Passive manipulations were performed at least 60 minutes after drug administration to allow for drug absorption. Passive manipulations were conducted through the flexion and extension of several joints including the wrist, elbow, shoulder (abduction/adduction), hip (abduction/adduction), knee, and ankle contralateral to the STN and GPi DBS implants.

Subject F experiment

Subject F was part of a 15-day study to investigate coordinated reset therapy with STN-DBS, with the last two days devoted to investigating clinical STN-DBS therapy. There was no L-Dopa given to the animal during the study and two types of STN-DBS stimulation approaches were tested in the context of rigidity measurements. The two types of STN-DBS used were "coordinated reset" STN-DBS and high-frequency clinical STN-DBS. For coordinated reset, the DBS contacts are randomly stimulated in different bipolar configurations. For the clinical STN-DBS, contacts 1 and 2 were used to stimulate at an amplitude of 1V with 120 μs pulse width at 130 Hz. Passive manipulations were conducted through the abduction and adduction of the shoulder contralateral to the STN-DBS implant at multiple time points during the session: baseline, 30 min during stimulation, 90 min during stimulation, 30 min post-stimulation, and 60 min post-stimulation. The schedule for the 15-day study was as follows: Days 1-5 were assigned as uncoordinated reset DBS trials, Days 6-13 were assigned to no stimulation and Days 14 and 15 were assigned to clinical DBS. For the days with no stimulation, baseline data was still collected at the same time intervals as the days with stimulation, to keep the protocol consistent. The rigidity measuring device testing with Subject F was used to observe device consistency within days and measuring relative changes across days to show the chronic effects post coordinated reset STN stimulation and the acute effect post clinical STN stimulation. Due to damage to the device early in the testing, only days 14 and 15 were usable for analyzing.

Data Analysis

All analysis was performed offline in Matlab (v2012b, Natick MA). See Appendix 2 for the analysis code. The differential force signal from the load cells and the position signals were low-pass filtered (fifth order butterworth, cutoff 12.5 Hz). For each trial, the first and last ten seconds of movements were removed to allow for analysis of movements that are consistent and when the animal is most relaxed. The angle was then calculated using the law of cosines.

Equation 1: $$c^2 = a^2 + b^2 - 2ab\cos\theta$$

Since the position of the three markers is measured with the infrared camera systems, the equation can be re-arranged to solve for theta:

Equation 2: $$\theta = \cos^{-1}\frac{a^2+b^2-c^2}{2ab}$$

Using the angle data, extension and flexion segments were calculated by detecting the direction of angle changes. Each juxtaposed flexion and extension was combined serially as one movement. Principal component analysis was conducted on the angle data, using a cluster algorithm in Matlab, to reject outlier movements that may have resulted from voluntary movement during the recording session. The cluster analysis was performed with nominally five group designations; however, this number was adapted manually according to the number of visually unique outliers. The unit on the sensor data output as voltage into Matlab (for Subject P) or Motion Analysis (for Subject F) was converted to force (newton) using the calibration curves (see Figure 7). The areas for each movement were defined by first plotting the extension and flexion manipulations on a Force vs. Angle plot, and then calculating the area between the flexion and extension curves and subtracting the two areas to find the area between the two curves.

For statistical comparisons, non-parametric tests were conducted due to the small sample size of each trial and the lack of normally distributed data. More specifically the Kruskal-Wallace test with a significance level of $p<0.05$ was performed to show significance among different trials since each trial could have variable sample sizes. Additionally, the desire to compare more than two groups requires the Kruskal-Wallace test, since the test is a one way analysis of variance. The Dunn test for multiple comparisons was conducted post-hoc for each data set that rejected the null hypothesis for the Kruskal-Wallace test. If the null hypothesis for the Dunn test was rejected, this was indicated by significance bars in each of the graphs ($p<0.05$).

Results

Arduino and NI-DAQ calibration

As mentioned in the methods, a calibration device was built to translate voltage output from the load cells to actual force applied (Figure 5). Since the Arduino and the

NI-DAQ had different input currents, load cells were calibrated in both DAQ set-up was recorded separately (Figure 7). With $R^2 > 0.99$ for all calibration curves, there was high confidence going forward that the load cell voltage would correctly converted into the unit of newton.

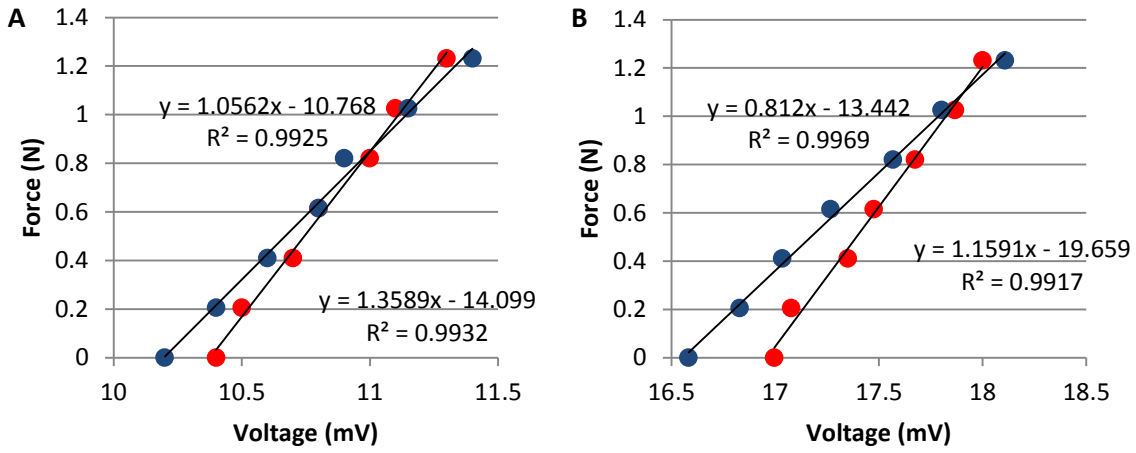

Figure 7: Calibration Curves. Calibration fits for sensor01 (blue) and sensor02 (red) for both A) Arduino and B) Motion Analysis set-ups.

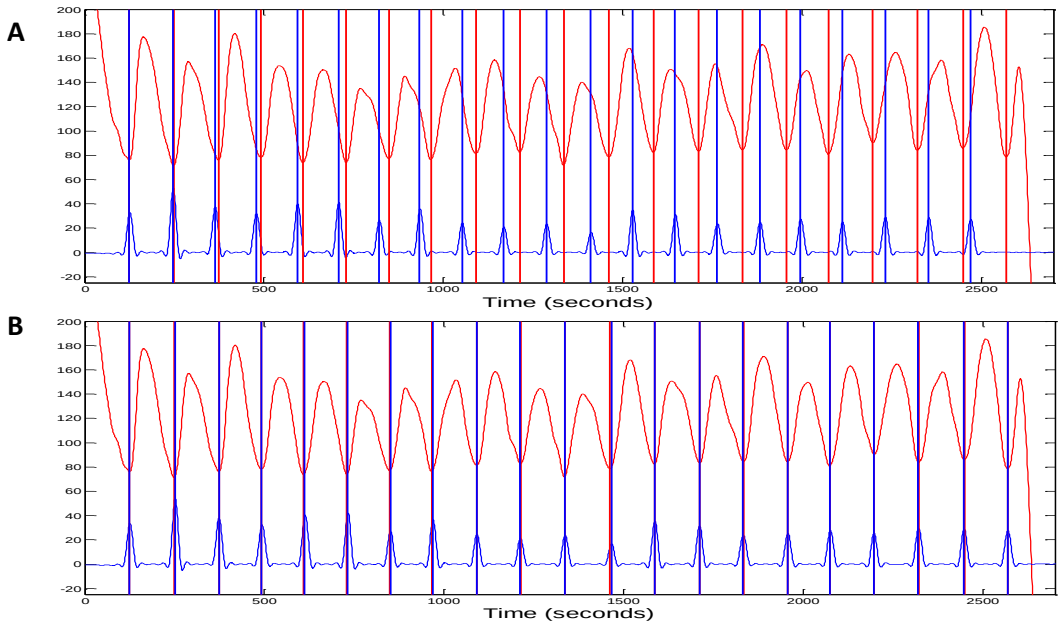

Figure 8: Arduino Lag Calculation. Load cell output voltage (blue) and infrared camera position data (red) with A) lagged voltage data and B) resampled load cell voltage data.

Lag component in Arduino DAQ

When analyzing the data from Subject P the voltage data from the load cells did not align well between the position data from the infrared camera system. In the Arduino set-up, there was a pulse sent from the camera system to the Arduino (see Figure 2C methods) to sync the load cell and position data. Even with the sync pulse, the position data seemed to lag consistently behind the voltage data (Figure 8A). To correct for this delay, the load cell data was resampled with a frequency of 1.0425 Hz (Figure 8B).

Sensor Performance

Before testing with the NHPs, the load cells were tested on a healthy human elbow to ensure the sensor differential set-up would capture changes in rigidity. The load cells were tapped onto a healthy human forearm, with the sensing tip pointing out from the limb, as not to cause discomfort. The two states captured were passive manipulation of the elbow (Figure 9A), and actively resisting elbow joint articulation (Figure 9B), used as an approximate surrogate of rigidity. Average area and standard deviation of the force-angle curves were calculated and compared (Figure 9C,D). There was 145% difference in normalized area (defined by the area between extension and flexion force-angle curves, divided by the number of degrees used in the joint articulation) calculated between the resistive state and the passive state. Through one-way Kruskal-Wallace test, the null hypothesis was rejected meaning the two states were from different sample populations ($p= 0.0223$).

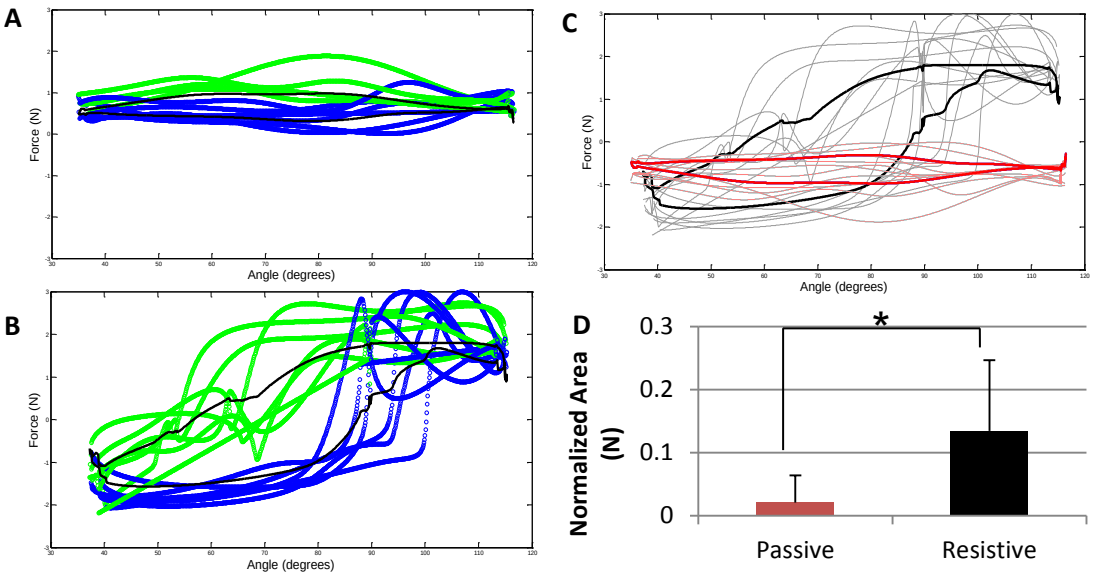

Figure 9: Sensor Performance – Resistive vs. Passive. Extension (green) and flexion (blue) force-angle curves, with the average curve (black) for A) passive state and B)resistive state. C) Shows the passive (red) and resistive (black) state trials plotted on the same axes D) Normalized area for passive state (red) and resistive state (black) with standard deviation bars being displayed.

Device 1 - Validation testing

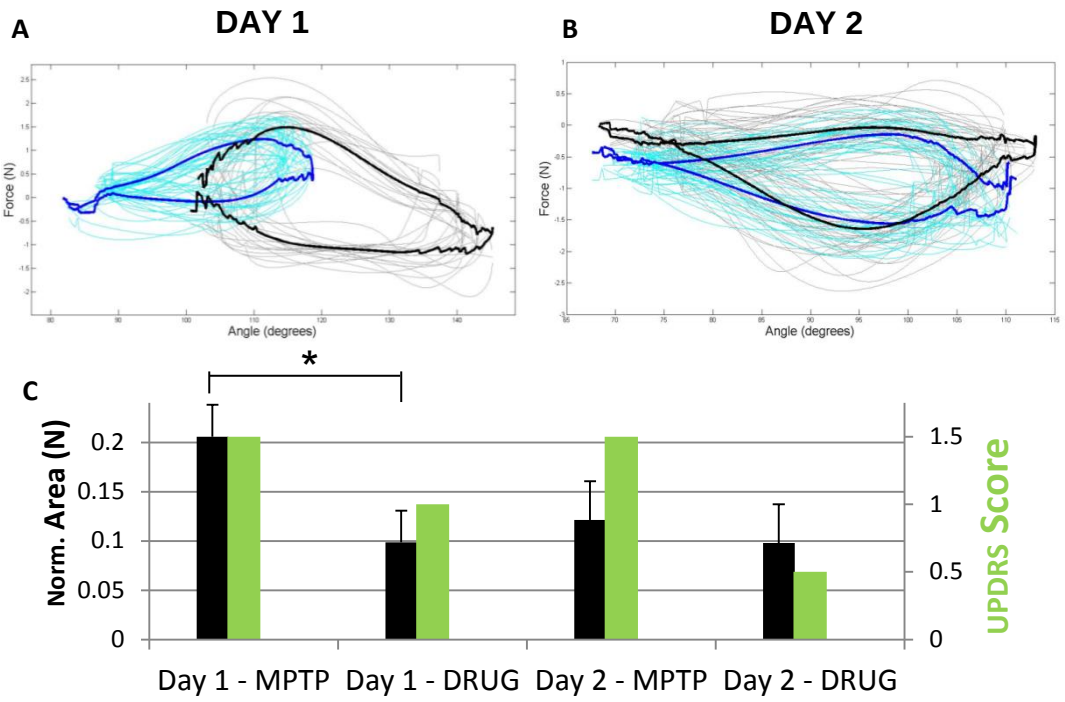

Figure 10: Device 1 Validation. Force-angle curves for MPTP (grey) and DRUG (cyan) knee joint trials, with the average force-angle for each plotted in bold (black for MPTP, blue for DRUG) for A) Day 1 and B) Day 2. C) Normalized areas from the average force-angle curve (black) compared with the UPDRS Score (green) that the experimenter qualitatively determines.

During the two-day testing of device 1, Subject P was tested in both the rigid MPTP state and drug treated state (Sinemet, 150 mg). The force-angle plots for the MPTP and drug trials for both day 1 (Figure 10A) and day 2 (Figure 10B) reflect the consistent curves within a day but less consistent curves between days. This partly stemmed from slightly different angles in which the experimenter used to articulate the joint, which in the case of Figure 4 was the knee. Thus, the area between the extention and flexion force-angle curves was normalized by the angle range (Figure 10C). By normalizing by the angle range, movements at different angle ranges could be compared. There was a 0.78% difference between the normalized area for the drug trials between days 1 and 2. Furthermore, there was a 70% decrease in normalized area between the MPTP and drug state from day 1, while there is only a 20% decrease for day 2. A one-way Kruskal-Wallace test was conducted on all four trials and, the null hypothesis was rejected meaning there are at least two different sample populations ($p = 2.2883e-18$) which could be interpreted as two different states.

Also plotted in Figure 10C are the UPDRS scores that the researcher assessed on Subject P prior to running the test with the device. Since the UPDRS scores are the standard for measuring rigidity, they will be used as a validation measure that the device was working properly and capturing appropriate level of rigidity. From Figure 10C, it seems that the relative changes in normalized area do not match the UPDRS scores directly, but rather follow similar trends. For example, the UPDRS scores decrease from the MPTP trials to the drug trials and the same can be seen in the normalized areas for both days.

Device 1 was captured data from six joints, including: the elbow, wrist, shoulder, hip, knee, and ankle from a parkinsonian non-human primate (Figure 11). As shown in Figure 11, the device was tested in three conditions, including MPTP, GPi-DBS, and Sinemet. The joint that showed the most consistency, based on average standard deviation of the normalized area across all three trials was the knee (± 0.0313) and the joint with the least consistency was the ankle (± 0.2943) with the wrist also showing a lack of characteristic force-angle curves. The slope of the flexion or extension was considered and analyzed, but the slopes did not correlate well with changes in rigidity

(data not shown). The plots shown in Figure 11 have the same axes as other trials on the same joint; therefore, the force data for the MPTP trial for hip was collected at a much different angle range than the GPi-DBS trial. While a difference in angle range length can be compensated for with normalization, the actual angle range at which the rigidity data was collected cannot be changed

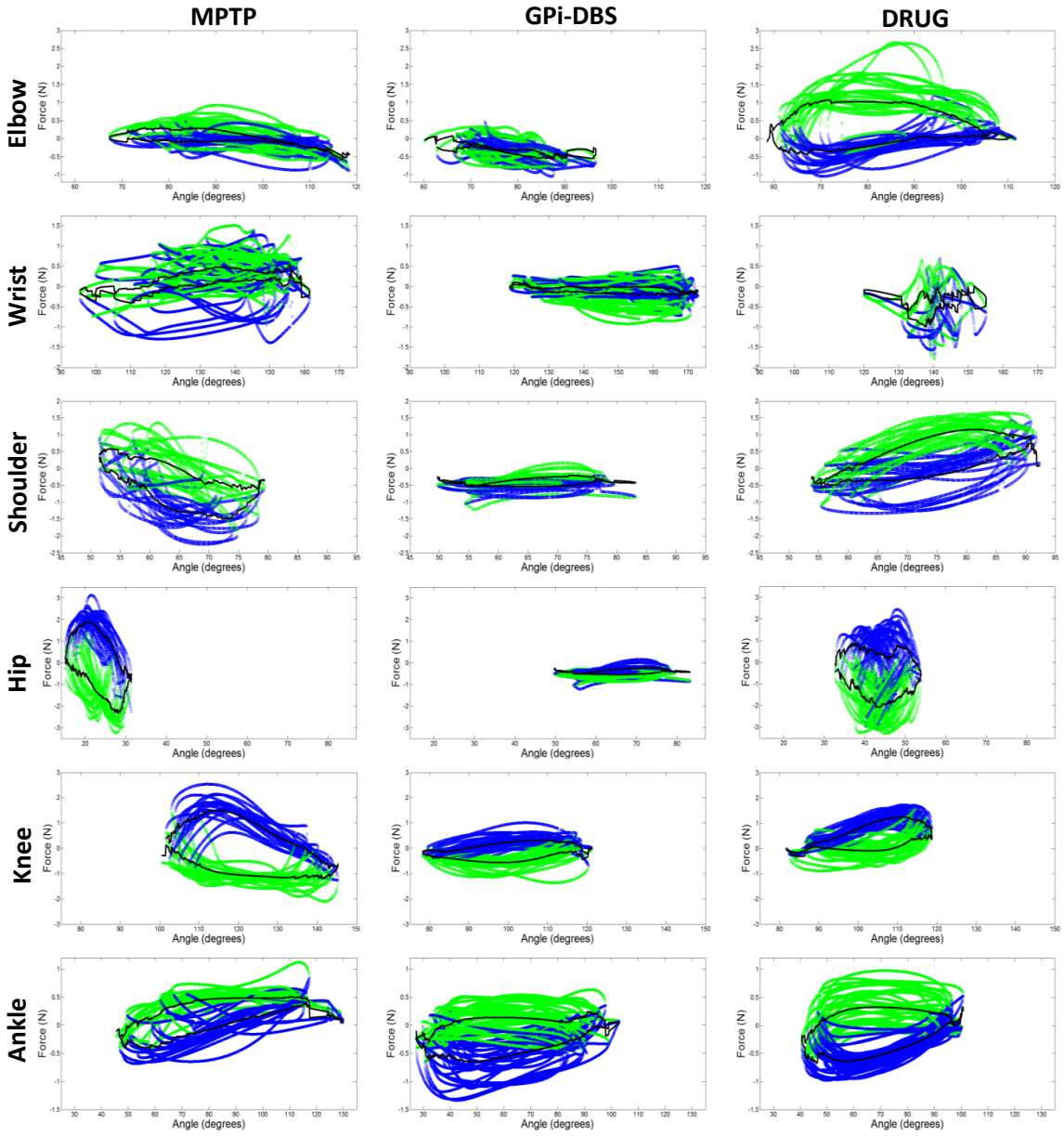

Figure 11: Device 1 multi-joint testing. Force-angle curves for MPTP, GPi-DBS, and drug trials across six different joints on Day 1. Extensions (green) and flexions (blue) were averaged (black) for each trial.

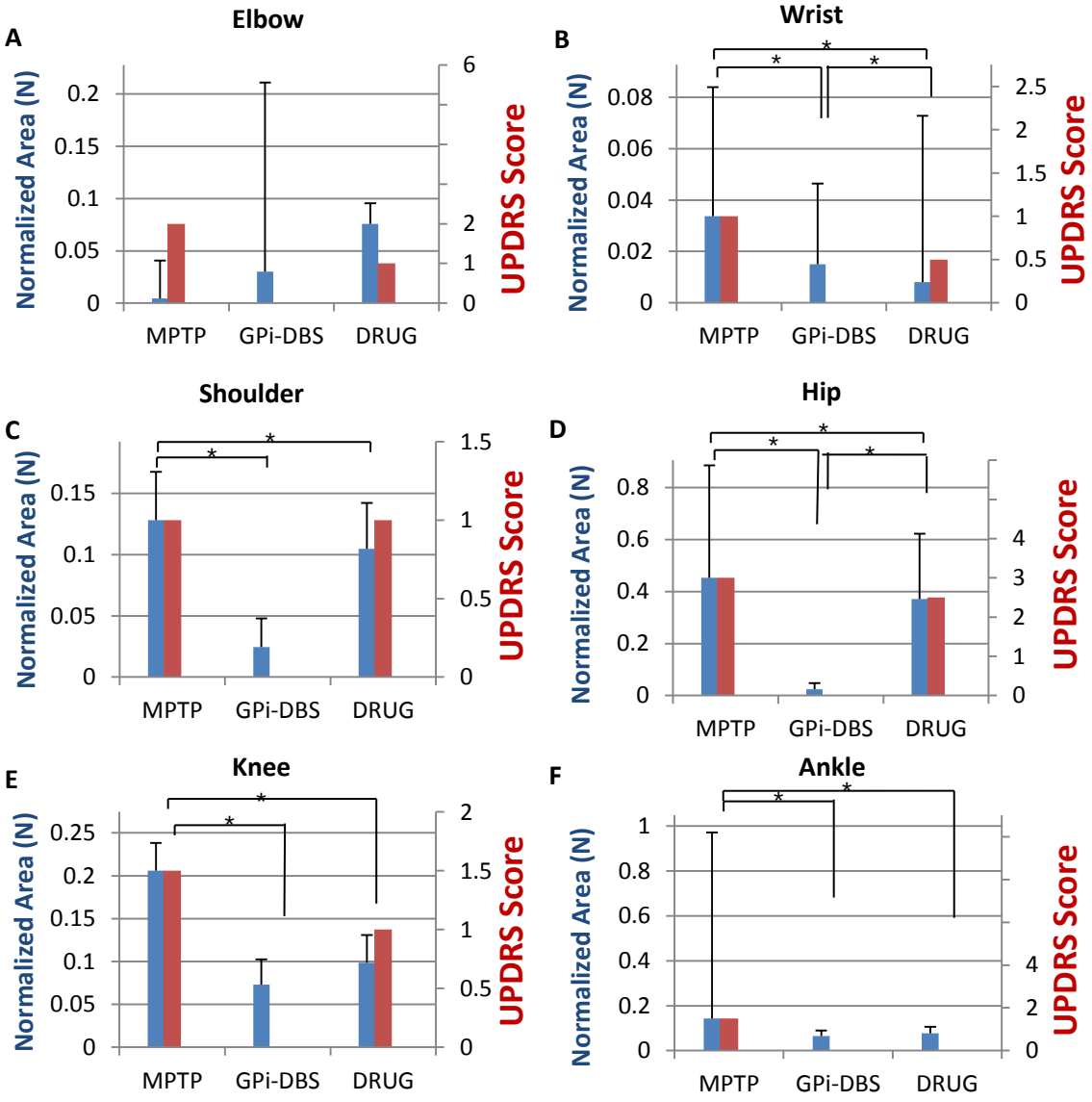

Figure 12: Device 1 multi-joint results. Comparing the normalized area (blue) and UPDRS scores (red) for MPTP, GPi-DBS, and drug states across all six joints.

Note that there was no UPDRS score taken before the GPi-DBS trials, so there is no UPDRS score to report. It should also be mentioned that the elbow MPTP trial was the first trial for the researcher, and there seemed to be a one trial learning curve for the researcher to become comfortable with the device, so there was no accurate MPTP data for the elbow. When comparing the UPDRS score to the normalized area for each trial, in general, the normalized area changes match well with the UPDRS scores. A one-way Kruskal-Wallace test was conducted on each joint trials and, the null hypothesis was

rejected for all of the joints: wrist (p=6.4410e-05), shoulder (p=1.2786e-11), hip (p=2.6660e-07), knee (p=1.1394e-10), and ankle (p=8.4770e-04) except the elbow, meaning device 1 was able to detect more than one population, or in this case rigidity state, among each joint.

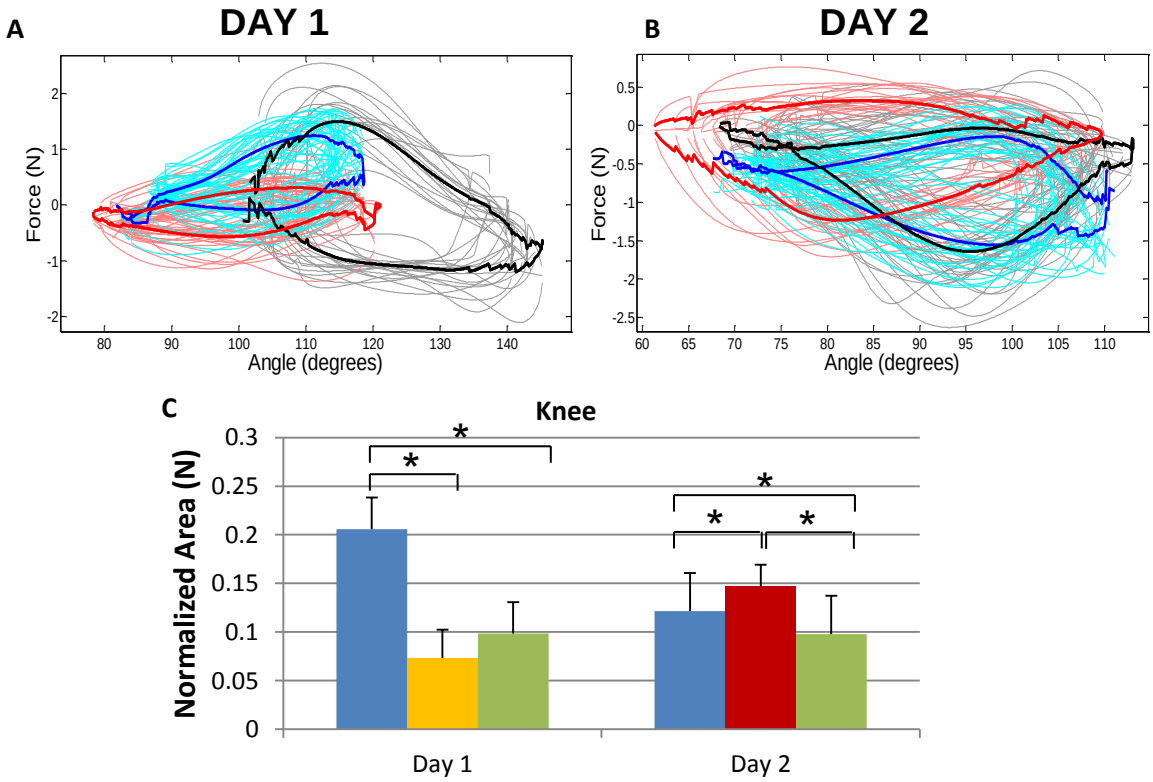

Figure 13: Device 1 comparing therapies. A) Force-angle curves for MPTP (black), GPi-DBS (red), and drug (blue) for the knee. B) Force-angle curves for MPTP (black), STN-DBS (red), and drug (blue). C) The normalized area calculated for MPTP (blue), drug (green) and either GPi-DBS (orange) and STN-DBS (red) trials with standard deviation bars.

From Figure 13C, there was a 95.1% decrease between the normalized area for the MPTP and GPi-DBS stimulation, while there was only a 70.4% decrease between the MPTP and drug trial for day 1. As for day 2, there was an 18.9% increase in normalized area between the MPTP and STN-DBS state and only a 21.5% decrease between the MPTP and drug trials. A one-way Kruskal-Wallace test was conducted on each day of trials and, the null hypothesis was rejected for each day (day1: p= 1.1394e-10; day 2: p=2.5112e-04), further supporting the detection of multiple rigidity states.

Device 2 – Validation Testing

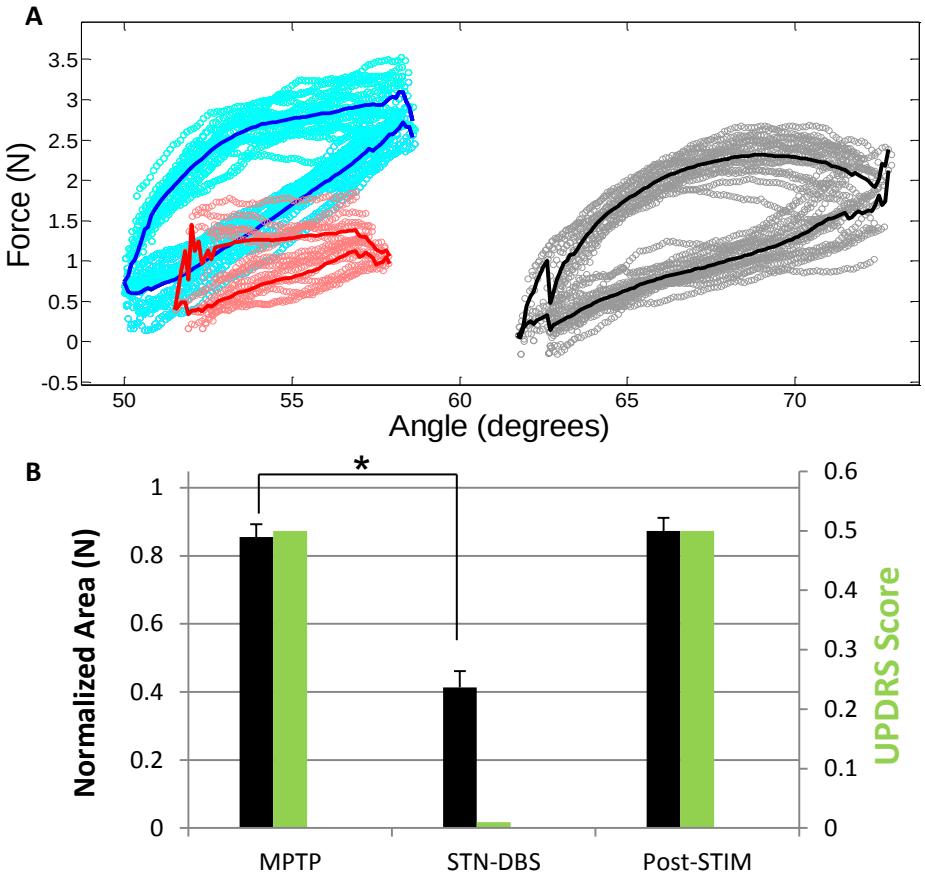

Figure 14: Device 2 Validation. A) Force-angle curves for MPTP (grey), STN-DBS (pink) and 30 minutes post-stimulation (cyan) shoulder joint trials, with the average force-angle for each plotted in bold (black for MPTP, red for STN-DBS, and blue for Post-STIM). B) Normalized areas from the average force-angle curve (black) compared with the UPDRS Score (green) that the experimenter qualitatively determines, standard deviation is plotted as error bars.

Subject F was tested in both the rigid MPTP state, during STN-DBS, and 30 minutes after STN-DBS (Post-STIM) for abduction and adduction to the shoulder joint. The force-angle plots for Day 14 of testing with Subject F is shown in Figure 14A and average normalized area with standard deviation was compared to the qualitative UPDRS Score in Figure 8B. In Figure 14A, there is a 4 degree gap between the Post-STIM trials and the MPTP trials. In Figure 8B, the area between the extention and flexion force-angle curves was normalized by the angle range. By normalizing by the angle range, movements at different angle ranges could be compared. There was a 69.7% decrease from the normalized area of the MPTP trials to the normalized area of the STN-DBS

trials. Furthermore, there was a 2.12% difference between the normalized area of the MPTP and Post-STIM states. A one-way Kruskal-Wallace test was conducted on all three trials and, the null hypothesis was rejected meaning there are at least two different sample populations ($p = 9.3043e-05$) which was be interpreted as two different states.

Discussion

This study involved the design of a rigidity measuring device and testing in parkinsonian NHPs. The system enabled quantitative measurement of joint resistance and has future potential for titrating PD therapies, including deep brain stimulation and dopamine replacement. In comparison to previous systems that measure muscle rigidity, the system described here provided a method to evaluate rigidity about multiple joints with a single device set-up that required minimal effort to transition amongst joints.

Device Interpretations

The main result from the recordings was the measurement of the area from the force-angle curves for each joint. The indicator for a change in rigidity was a significant increase or decrease in the area between the flexion and extension curves on the force-angle plots. These results have been found by several other papers (Caliguiri 1989, Caliguiri 1992, Dai 2013, Endo 2009, Fung 2000, Mera 2009). Other studies mention using the slope as a means to indicate a change in rigidity (Caliguiri 1994, Mera 2009). However, the measurements obtained in the parkinsonian non-human primates did not exhibit a consistent slope during extension and flexion phases of the movement. One possibility for this difference is that a rubber stopper placed at the base of the metal transducer hole in device 1 may have caused an elastic effect on the shape of the force-angle curves.

Device Ergonomics

When creating a device that interfaces directly with the user, ergonomics must be considered to allow for comfortable and efficient use of the device. The use of Velcro straps on both the experimenter's hand and the subjects' limbs proved to be effective at creating an adjustable and stable attachment method. For device 1, the adjustable loops

that were attached to the transducer allowed for efficient aligning of sensors before beginning a trial. While the ergonomics of the measuring device were a primary consideration in the design of the device, there were some limitations associated with each of the final designs. One limitation to both device was the height of the sensors, and the bulkiness it created when the researcher tried to grasp and manipulate the limb while wearing the device. Additionally, device 2 had 3-D printed caps that were not completely form-fitting, which resulted in pressure on the cap that was not necessarily being distributed entirely as a force in the direction tangential to the load cell button and instead may have resulted in torques. The 3-D printed cap over the load cell button also limited the area for the fingers to grasp, while in device 1 the load cells were directly attached with Velcro to the digits of the experimenter.

Device Durability

In addition to ergonomics, durability is another concern when building a device. Both device concepts had strengths and flaws in regard to durability. For device 1, the attachment of the load cells to the hand of the experimenter increased durability. The design allowed for the experimenter to pull the load cells away from the subject and avoid damage. A flaw in the device 1 design was in the attachment of the metal transducer interface. The transducer interface was sewn on to fabric loops. This posed a problem because after several trials under resistive forces, the stiches on the transducer began to loosen and ultimately fail. This failure was experienced when testing device 1 in Subject F. Device 2 had a more expensive durability issue. The caps that were placed on the sensing tip of the load cells had space between the cap and the sensing unit so the cap could be placed over the sensors. The problem with this space is that it caused the caps to become slightly unstable and teeter during the joint articulations. During the experimental sessions, the teetering to one side or the other on the load cell tip caused the tip to dislodge from the primary unit several times, ultimately failing due to unintended torques at the sensing tip. In addition, since device 2 was attached via velcro to the limb of the subject (not to the fingers of the experimenter), there was not enough time to pull the device away from the subject before damage to the sensor occurred. On the positive side, the 3D printed caps for device 2 were unaltered and maintained shape through torques.

Thus, the 3D printing materials and methods used to create the device 2 caps should be used in future 3D printing endeavors.

Sources of Error

After completing the studies, there were several aspects of the study where more information would have been helpful and a more strict protocol would have supported a better result. One such change in the protocol would be the placement of sensors. One idea could be to keep the Velcro strap on the subject for the whole trial period for the day and see if that could improve the intra-day variance in trials. The way the testing was done in the study, the Velcro straps were taken on and off between the trials and moved around to the limb of interest. While the straps were returned close to the previous spot, there was most likely some error in placing and replacing the straps between days.

The device 1 and 2 both followed the UPDRS score fairly well but there were a few cases where differences existed. One source of error could stem from the fact that the UPDRS was not recorded simultaneously when the rigidity was measured by the device. This was mostly due to the fact that it was easier to record the UPDRS all at once and then record the rigidity via the device. The reason why this might be a concern is for the drug trials. With more time elapsed before testing the rigidity device, there was more time for the absorption of the drug. This could cause further reduction in rigidity relative to the UPDRS score taken minutes before.

Since the rigidity measurement experiments were not the main studies for each NHP, the testing of the rigidity measurement device was limited. Subjects that have been trained for passive manipulation, implanted with DBS leads and induced parkinsonian, were sparse therefore explaining why testing was limited. With only two short studies being conducted with the devices, it is conceivable that with more testing, more information about these devices could be collected.

Several studies have mentioned using a surface EMG to detect if the subject is resisting or allowing passive manipulations (Endo 2009, Fung 2000, Mera 2009). For the current study, we were unable to add the EMG sensors to the protocols for Subject P and

Subject F due to the already dense protocols (Subject P) or limitations due to the study (Subject F). Having EMG sensors would be very important for future testing so that active resisting of the subject could be detected and the trial ruled out of analysis. In this study, the experimenter noted if they felt the subject resisting passive manipulation, which was qualitative and could lead to contradicting results.

A limitation of the load cells from Measurement Specialties was the lack of sensing in the tangential plane of the limb. The load cells could only detect in one direction, which was the force normal to the limb. An additional issue with the device was the lack of feedback for the experimenter to know what angle range was from the previous trials. The absence of feedback led to the angle range for different trials to be very different. The biggest problem with not having the same angle range is the muscle recruitment to achieve that movement at that angle range. Therefore even if the area is normalized by dividing the force-angle area by the angle range, this doesn't compensate for the fact that the different trials could be activating different muscles and measuring different joint rigidities.

Future Directions

Neither device 1 nor devices 2 are a finished product, but move along the path to a final working device that could have broad application to preclinical and clinical studies. To address an ergonomic concern, the next generation should have shorter load cells. While the Measurement Specialties load cell had the sensitivity and functionality to capture rigidity, the size of the sensors would limit a study if the NHP limbs were large or if the experimenter had small hands.

Device 1 had durability issues with the transducer interface, while device 2 had sensor durability problems. The set-up for device 1 would be the preferred orientation of the sensors given on feedback from testing. Device 1 set-up allows the experimenter to remove the device quickly from the subject, which is ideal working with NHPs. Therefore, improving the transducer interface of Device 1 would be the next direction to further improve this device. If the interface of the transducer for device 1 is 3D printed with two plastic brackets on either side of the transducer interface, then Velcro could be

looped through the brackets, similar to a belt, and the transducer would have a specific-size 3D printed opening for the load cell tip to lock into the transducer interface. This would take the best aspects from both device 1 and device 2. Also for future studies, it would be ideal to make at least two sets of transducers since two different lengths of Velcro were used to adjust to the lower limbs vs the upper limbs / distal joints.

The next generation device should incorporate a way to track angle changes online, since the variability in angle ranges across trials was a major limitation to this study. The joints that had the most consistent area calculations were the joints that had the most consistent angle ranges across different days and therapeutic states. With the current set-up, the experimenter was expected to manipulate the limb of interest in the most accurate and consistent manner possible, as to capture a consistent angle. That tactic seemed to fair well within the same trial. But between trials, it would be very difficult for the experimenter to know the exact angle range that they tested an hour before. The rigidity changes in the joint from a therapy condition could further complicate the experimenter's memory of the movement previously performed. To alleviate this problem, the experimenter would need feedback from the infrared camera system. This could be achieved by streaming the data from the infrared cameras into Matlab and displaying the angle calculation in a Matlab GUI. In addition, an audio feedback could be used. The experimenter could wear head phones that would emit a frequency based position method, where the frequency of the sound will change as the experimenter changes the angle of the limb, and the experimenter would listen to stay within a range of frequencies.

Conclusion

The objective of this research was to build an accurate, inexpensive, and easy-to-use rigidity measurement tool to quantifying parkinsonian rigidity. The results indicate that the rigidity-testing device presented here is sensitive enough to measure changes in rigidity resulting from dopamine replacement and DBS therapies. Furthermore, the unique handheld differential load cell design allows for testing of multiple joints (wrist, elbow, shoulder, ankle, knee, hip) and has potential to be extended further.

Currently, clinicians use UPDRS to measure rigidity in Parkinson's disease patients, but the scale has a small range and is subjective to inter-clinician variability. Future iterations of this rigidity testing device could be used in the clinic to assist neurologists in titrating medication levels and DBS parameters. However, future iterations will also need to address several limitations of the current device, including the inability to quantify transverse torque at the point of contact of the sensor, confounding forces due to the subject actively resisting during manipulations, and possible variability in measurement due to inconsistent placement of the sensors on the subject's limbs between trials.

References

Brown RA, Lawson DA, Leslie GC, Macarthur A, Maclennan WJ, McMurdo MET, Mutch WJ, Part NJ. Observations on the applicability of the Wartenberg pendulum test to healthy, elderly subjects. *Journal of Neurology, Neurosurgery and Psychiatry* 51.9:1171-1177, 1988.

Chan HC, Manry MT, and Kondraske GV. Classification of resistance to passive motion using minimum probability of error criterion. *Annals of biomedical engineering* 15.6: 579-590, 1987.

Caligiuri MP, Bracha HS, and Lohr, JB. Asymmetry of neuroleptic-induced rigidity: development of quantitative methods and clinical correlates. *Psychiatry research* 30.3: 275-284, 1989.

Caligiuri MP, and Galasko DR. Quantifying drug-induced changes in parkinsonian rigidity using an instrumental measure of activated stiffness. *Clinical neuropharmacology* 15.1:1-12, 1992.

Caligiuri MP. Portable device for quantifying parkinsonian wrist rigidity. *Movement disorders* 9.1:57-63, 1994.

Cano-de-la-Cuerda R, Vela-Desojo L, Miangolarra-Page JC, Macías- Macías Y, Muñoz-Hellín E. Axial rigidity and quality of life in patients with Parkinson's disease: a preliminary study. *Quality of Life Research* 20.6:817-823, 2011.

Chiba S, Takada E, Tadokoro M, Taniguchi T, Kadoyama K, Takenokuchi M, Kato S, Suzuki N. Loss of dopaminoreceptive neuron causes L-dopa resistant parkinsonism in tauopathy. *Neurobiology of Aging* 33.10: 2491-2505, 2012.

Dai H, Otten B, Mehrkens JH, D'Angelo LT. A portable system for quantitative assessment of parkinsonian rigidity. *IEEE Engineering in Medicine and Biology Society Conference Proceedings 2013*:6591-6594, 2013.

Delwaide, PJ. Parkinsonian rigidity. *Functional Neurology* 16.2: 147-156, 2001.

Endo T, Okuno R, Yokoe M, Akazawa K, Sakoda S. A novel method for systematic analysis of rigidity in Parkinson's disease. *Movement disorders* 24.15: 2218-2224, 2009.

Fox SH, and Brotchie JM. The MPTP-lesioned non-human primate models of Parkinson's disease. Past, present, and future. *Prog Brain Res* 184:133-157, 2010.

Fung VS, Burne JA, and Morris JG. Objective quantification of resting and activated parkinsonian rigidity: a comparison of angular impulse and work scores. *Movement disorders* 15.1:48-55, 2000.

Galvan A, and Wichmann T. Pathophysiology of parkinsonism. *Clinical neurophysiology* 119.7:1459-1474, 2008.

Hong M, Perlmutter JS, and Earhart GM. Enhancement of rigidity in Parkinson's disease with activation. *Movement disorders* 22.8:1164-1168, 2007.

Imbert C, Bezard E, Guitraud S, Boraud T, Gross. Comparison of eight clinical rating scales used for the assessment of MPTP-induced Parkinsonism in the Macaque monkey. *J Neuroscience Methods* 96:71–6, 2000.

Johnson MD, Miocinovic S, McIntyre CC, Vitek JL. Mechanisms and targets of deep brain stimulation in movement disorders. *Neurotherapeutics* 5.2:294-308, 2008.

Kondraske GV, Potvin AR, Tourtellote WW, and Syndulko K. A Computer-Based System for Automated Quantitation of Neurologic Function. *IEEE Transactions on Biomedical Engineering* 31.5:401-414, 1984.

Lakie M, Walsh EG, and Wright GW. Resonance at the wrist demonstrated by the use of a torque motor: an instrumental analysis of muscle tone in man. *Journal of Physiology* 353:265-285, 1984.

de Lau LM, Giesbergen PC, de Rijk MC, Hofman A, Koudstaal PJ, Breteler MM. Incidence of parkinsonism and Parkinson disease in a general population: the Rotterdam Study. *Neurology* 63:1240–1244, 2004.

Levin J, Krafczyk S, Valkovic, Eggert T, Claassen J, Botzel K. Objective measurement of muscle rigidity in Parkinsonian patients treated with subthalamic stimulation. *Movement Disorders* 24.1:57-63, 2009.

Little S, Joundi RA, Tan H, Pogosyan A, Forrow B, Joint C, Green A, Aziz TZ, Brown P. A torque-based method demonstrates increased rigidity in Parkinson's disease during low-frequency stimulation. *Experimental Brain Research* 219.4: 499-506, 2012.

Long C, Thomas D, Crochetiere WS. Objective measurement of muscle tone in the hand. *Clinical Pharmacological Therapy* 5: 909–917, 1964.

Louis ED, Tang MX, Cote L, Alfaro B, Mejia H, Marder K. Progression of parkinsonian signs in Parkinson disease. *Archives of Neurology* 56.3: 334-337, 1999.

Mak MK, Wong EC, and Hui-Chan CW. Quantitative measurement of trunk rigidity in parkinsonian patients. *Journal of neurology* 254.2:202-209, 2007.

Meara RJ, and Cody FW. Stretch reflexes of individual parkinsonian patients studied during changes in clinical rigidity following medication. *Electroencephalography and clinical neurophysiology* 89.4:261-268, 1993.

Mera TO, Johnson MD, Rothe D, Zhang J, Xu W, Ghosh D, Vitek J, Alberts JL. Objective quantification of armrigidity in MPTP-treated primates. *Journal of Neuroscience Methods*, 177(1):20-9, 2009.

Niazmand K, Tonn K, Kalaras A, Fietzek UM, Mehrkens JH, Lueth TC. Quantitative evaluation of Parkinson's disease using sensor based smart glove. *IEEE Computer Society Press*, (Los Alamitos, California): 1-8, 2011.

Nussbaum RL, and Ellis CE. Alzheimer's disease and Parkinson's disease. *The New England Journal of Medicine* 348.14:1356-1364, 2003.

Park BK, Kwon Y, Kim J, Lee J, Eom G, Koh S, Jun J, Hong J. Analysis of viscoelastic properties of wrist joint for quantification of parkinsonian rigidity. *IEEE Transactions on Neural Systems and Rehabilitation Engineering* 19.2:167-176, 2011.

Patrick SK, Denington AA, Gauthier MJA, Gillard DM, Prochazka A. Quantification of the UPDRS Rigidity Scale. *IEEE Transactions on Neural Systems and Rehabilitation Engineering* 9(1):31-41, 2001.

Prochazka A, Bennett DJ, Stephens MJ, Patrick SK, Sears-Duru, Roberts T, Jhamandas JH. Measurement of rigidity in Parkinson's disease. *Movement Disorders* 12(1):24-32, 1997.

Rätsep T, and Asser T. Changes in viscoelastic properties of skeletal muscles induced by subthalamic stimulation in patients with Parkinson's disease. *Clinical Biomechanics* 26.2: 213-217, 2011.

Relja MA, Petravic D, and Kolaj M. Quantifying rigidity with a new computerized elbow device. *Clinical Neuropharmacology* 19.2:148-156, 1996.

Schrag A, Quinn N. Dyskinesias and motor fluctuations in Parkinson's disease. A community-based study. *Brain* 123: 2297–2305, 2000.

Sepehri B, Esteki A, Ebrahimi-Takamiani E, Shahidi G, Khamseh, Moinodin M. Quantification of rigidity in Parkinson's disease. *Annals of Biomedical Engineering* 35.12: 2196-2203, 2007.

Shapiro MB, Vaillancourt DE, Sturman MM, Metman LV, Bakay RAE, and Corcos DM. Effects of STN DBS on rigidity in Parkinson's disease. *IEEE Transactions on Neural Systems and Rehabilitation Engineering* 15.2:173- 181, 2007.

Van Dillon LR, Roach KE. Inter-rater reliability of a clinical scale of rigidity. *Phys Ther* 68:1679-81, 1988.

Vu TC, Nutt JG, and Holford NH. Progression of motor and nonmotor features of Parkinson's disease and their response to treatment. *British Journal of Clinical Pharmacology* 74.2:267-283, 2012.

Watts RL, Wiegner AW, Young RR. Elastic properties of muscles measured at the elbow in man. II. Patients with parkinsonian rigidity. *JNNP* 49:1177-81, 1986.

Webster DD. A method of measuring the dynamic characteristics of muscle rigidity strength and tremor in the upper extremity. *IRE Trans Med Electron* ME 6:159-64, 1959.

Webster DD. Rigidity in extrapyramidal disease. *J Neurosurgery* 24:299-307, 1966.

Xia R, and Rymer WZ. The role of shortening reaction in mediating rigidity in Parkinson's disease. *Experimental Brain Research* 156.4:524-528, 2004.

Xia R, and Mao ZH. Progression of motor symptoms in Parkinson's disease. *Neuroscience Bulletin* 28.1:39-48, 2012.

Appendix 1: Hand Ergonomics

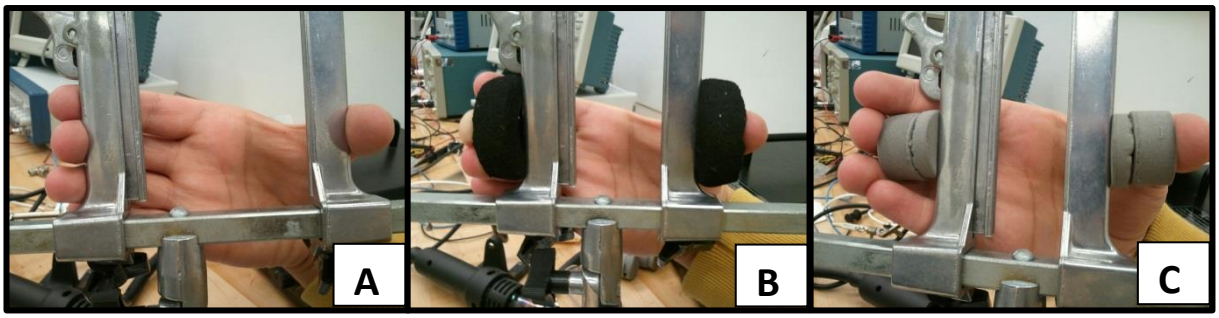

Figure 15: Hand grip measurements. Hand gripping measurements for A) no sensors B) black foam sensors C) grey foam sensors. The measured distance was between the outside edges of the two calipers.

Table 3: Hand grip test results

Set-up	Avg. distance between calipers	Notes
no sensors	13.36cm	-
black foam sensors	9.27 cm	Difficult not to torque the foam sensors with large interface
grey foam sensors	8.58 cm	Less stable than black foam sensors

grey foam sensors – diameter = 25 mm, height = 22 mm
black foam sensors – diameter = 45 mm, height = 16 mm

Conclusions: The height of sensors can be in the 22mm range, and the larger the diameter of the sensor the better, as it provides more stability for gripping.

Appendix 2 – Matlab Code

```
% ---------------------------------------------------------
%
% interpvicon.m
%
% Created by: Kevin Mohsenian
% Updated: 07-27-2014
%
% Description: Code that creates force-angle variables
%   over a specified time window of interest.
%
% ---------------------------------------------------------


%% Define markers based on the raw data

A=Peach2013102543;

marker(1).label = 'shoulder';
marker(1).x = A(:,3);
marker(1).y = A(:,4);
marker(1).z = A(:,5);

marker(2).label = 'elbow';
marker(2).x = A(:,6);
marker(2).y = A(:,7);
marker(2).z = A(:,8);

marker(3).label = 'wrist';
marker(3).x = A(:,9);
marker(3).y = A(:,10);
marker(3).z = A(:,11);

fs_marker = 100; % sampling rate
t_marker = [0:length(marker(1).x)-1]/fs_marker;

% Interpolate NaN points
for i=1:3
    marker(i).x = interp1(t_marker,marker(i).x,t_marker,'spline');
    marker(i).y = interp1(t_marker,marker(i).y,t_marker,'spline');
    marker(i).z = interp1(t_marker,marker(i).z,t_marker,'spline');
end

%% Plot positions in 3D space

% Define time of interest to plot
t_interest = 1:(length(t_marker)-300);
figure;
plot3(marker(1).x(t_interest),marker(1).y(t_interest),marker(1).z(t_int
erest),'Color',[0.6,0.6,0.6]); hold on
plot3(marker(2).x(t_interest),marker(2).y(t_interest),marker(2).z(t_int
erest),'Color',[0.6,0.6,0.6]);
```

```
plot3(marker(3).x(t_interest),marker(3).y(t_interest),marker(3).z(t_int
erest),'Color',[0.6,0.6,0.6]);

% Define the time window of interest
LowerBnd=1000;
UpperBnd=4000;

% 20: 1000-5500
% 32: 2100-4000
% 51: 1800-4800

% Run vicon analyze code to obtain angle / force variables
output = viconanalyze(sensor01,sensor02,sensor03,marker);
signal = output.signal(LowerBnd:UpperBnd);
resamp = output.ang(LowerBnd:UpperBnd);
figure; plot(resamp,signal);


function output = viconanalyze(sensor01,sensor02,sensor03,marker)

% Calculate the joint angle from the law of cosines
shoulder = [marker(1,1).x(:) marker(1,1).y(:) marker(1,1).z(:)];
elbow = [marker(1,2).x(:) marker(1,2).y(:) marker(1,2).z(:)];
wrist = [marker(1,3).x(:) marker(1,3).y(:) marker(1,3).z(:)];
shoulderelbow = distcalc3(shoulder,elbow);
elbowwrist = distcalc3(elbow,wrist);
wristshoulder = distcalc3(wrist,shoulder);
ang = 180/pi*acos(-(wristshoulder.^2 - elbowwrist.^2 -
shoulderelbow.^2)./(2*elbowwrist.*shoulderelbow));

% Upsample force sensor data
sensor01 = interp(sensor01,2);
sensor02 = interp(sensor02,2);
sensor03 = interp(sensor03,2);

% Convert sensor voltage to N
sensor01=(0.1359*sensor01)-14.099;
sensor02=(0.1072*sensor02)-10.935;

% Resample the sensor data to adjust for timing issue of the Arduino
start_time = find(sensor03>500,1);
end_time = length(sensor03);
anglewin = start_time:end_time;

% Synchronize Vicon measurements with sensor data
difference=sensor01(anglewin)-sensor02(anglewin);
ind=1:(length(difference));
for i=2:(length(difference))
    ind(i)=ind(i-1)+1.0425;
end
difference2=resample(difference,10425,10000);

% Filter the angle and force data
```

```
[b,a] = butter(5,8/100,'low');
signal=filtfilt(b,a,difference2);
ang1=filtfilt(b,a,ang);

% Assign output variables
A=[length(ang),length(signal),length(ind)];
mini=min(A);
output.ang=ang1(1:mini);
output.signal=signal(1:mini);
output.ind=ind(1:mini);

% Plot the reformatted data
figure; plot(output.ang/10-9,'b'); hold on; plot(output.signal,'r');
figure; plot(output.ang,'b'); hold on; plot(sensor01(anglewin),'m');
plot(sensor02(anglewin),'g');

end

function dist = distcalc3(pt1,pt2)
    dist = sqrt((pt1(:,1)-pt2(:,1)).^2+(pt1(:,2)-
pt2(:,2)).^2+(pt1(:,3)-pt2(:,3)).^2);
end


% ---------------------------------------------------------
%
% rigidityanalysis.m
%
% Created by: Kevin Mohsenian
% Updated: 07-27-2014
%
% Description: Code that analyzes the force-angle variables
%   and creates the appropriate plots.
%
% ---------------------------------------------------------

%clear; clc;
%load Trial3wVICON20_Peach_102613_analysis.mat;
%load Trial11wVICON32_Peach_102613_analysis.mat;
%load Trial17wVICON51_Peach_102613_analysis.mat;


%% Define variables
extct = 1; flxct = 1; k = 1; j = 1;
threshold = 0;


%% Define periods of joint articulation (e.g. extension-flexion)
for i = 2:length(resamp)-1,
    if resamp(i+1)-resamp(i) > threshold && resamp(i)-resamp(i-1) <
threshold,
        extct = 1;
        ext(j).data(extct,1) = resamp(i);
```

```
        ext(j).data(extct,2) = signal(i);
        extct = extct + 1;
        ext_index(j) = i;
        j = j + 1;
    end
    if resamp(i+1)-resamp(i) > threshold && resamp(i)-resamp(i-1) >
threshold,
        ext(j).data(extct,1) = resamp(i);
        ext(j).data(extct,2) = signal(i);
        extct = extct + 1;
    end
    if resamp(i+1)-resamp(i) < threshold && resamp(i)-resamp(i-1) >
threshold,
        flxct=1;
        flx(k).data(flxct,1) = resamp(i);
        flx(k).data(flxct,2) = signal(i);
        flxct = flxct + 1;
        flx_index(k) = i;
        k = k + 1;
    end
    if resamp(i+1)-resamp(i) < threshold && resamp(i)-resamp(i-1) <
threshold,
        flx(k).data(flxct,1) = resamp(i);
        flx(k).data(flxct,2) = signal(i);
        flxct = flxct + 1;
    end
end



%% Find the angle for which the flex and extend overlap

% Interpolate the extension data and define the min/max extension
angles
min_extangle = 180;
max_extangle = 0;
for i=2:length(ext)-1,
    TF=isempty(ext(i).data);
    if TF==1
        i=i+1;
    elseif length(ext(i).data)<10
        i=i+1;
    end
    extinterp(i).data(:,1) =
ceil(min(ext(i).data(:,1))*10)/10:0.1:floor(max(ext(i).data(:,1))*10)/1
0;
    extinterp(i).data(:,2) =
interp1(ext(i).data(:,1),ext(i).data(:,2),extinterp(i).data(:,1));
    if min_extangle > min(extinterp(i).data(:,1)),
        min_extangle = min(extinterp(i).data(:,1));
    end
    if max_extangle < max(extinterp(i).data(:,1)),
        max_extangle = max(extinterp(i).data(:,1));
    end
end
```

```
% Interpolate the flexion data and define the min/max flexion angles
min_flxangle = 180;
max_flxangle = 0;
for i=2:length(ext)-1,
    flxinterp(i).data(:,1) =
ceil(min(flx(i).data(:,1))*10)/10:0.1:floor(max(flx(i).data(:,1))*10)/1
0;
    flxinterp(i).data(:,2) =
interp1(flx(i).data(:,1),flx(i).data(:,2),flxinterp(i).data(:,1));
    if min_flxangle > min(flxinterp(i).data(:,1)),
        min_flxangle = min(flxinterp(i).data(:,1));
    end
    if max_flxangle < max(flxinterp(i).data(:,1)),
        max_flxangle = max(flxinterp(i).data(:,1));
    end
end

% Define a matrix containing all of the full articulation cycles
totalangle =
length([min_extangle:0.1:max_extangle,fliplr(min_flxangle:0.1:max_flxan
gle)]);
ang_matrix = ones(totalangle,min(length(extinterp)-2,length(flxinterp)-
2));
mov_matrix = NaN(totalangle,min(length(extinterp)-2,length(flxinterp)-
2));
for i=1:size(ang_matrix,2),
    TF=isempty(extinterp(i+1).data);
    if TF==1
        i=i+1;
    end
    ang_matrix(:,i) =
[min_extangle:0.1:max_extangle,fliplr(min_flxangle:0.1:max_flxangle)]';
    ind = find(abs(ang_matrix(:,i)-extinterp(i+1).data(1,1))<10^-6,1);
    mov_matrix(ind:length(extinterp(i+1).data(:,1))+ind-1,i) =
extinterp(i+1).data(:,2);
    ind = find(abs(ang_matrix(:,i)-flxinterp(i+1).data(end,1))<10^-
6,1,'last');
    mov_matrix(ind:length(flxinterp(i+1).data(:,1))+ind-1,i) =
flipud(flxinterp(i+1).data(:,2));
end


%% Cluster analysis

% Define variables
numtypes = 5;

% Perform the PCA
[coeff,score] = pca(mov_matrix');
T = clusterdata(score,numtypes);

% Sort the cluster matrix into groups
for i = 1:numtypes,
```

```
    clustergrp(i).ind = find(T==i);
end

% Select the cluster with the largest number of indices
clustertype = 1;
for i = 1:numtypes,
    maxind = length(clustergrp(i).ind);
    if maxind > clustertype,
        clustertype = i;
    end
end
for i = 1:length(clustergrp(clustertype).ind),
    ext_new(i).data = extinterp(clustergrp(clustertype).ind(i)+1).data;
    flx_new(i).data = flxinterp(clustergrp(clustertype).ind(i)+1).data;
    ang_matrix_new(:,i) = ang_matrix(:,clustergrp(clustertype).ind(i));
    mov_matrix_new(:,i) = mov_matrix(:,clustergrp(clustertype).ind(i));
end

% Calculate the average force-angle waveform
ang_matrix_avg = mean(ang_matrix_new,2);
mov_matrix_avg = zeros(size(mov_matrix_new,1),1);
ctr = 1;
for i=1:size(mov_matrix_new,1),
    for j=1:size(mov_matrix_new,2),
        if ~isnan(mov_matrix_new(i,j))
            mov_matrix_avg(i) = mov_matrix_avg(i)+mov_matrix_new(i,j);
            ctr = ctr + 1;
        end
    end
    if mov_matrix_avg(i) == 0,
        mov_matrix_avg(i) = NaN;
    end
    mov_matrix_avg(i) = mov_matrix_avg(i)/ctr;
    ctr = 1;
end

% Plot the primary cluster group
for i = 1:numtypes,
    figure;
    for j = 1:length(clustergrp(i).ind),

plot(extinterp(clustergrp(i).ind(j)+1).data(:,1),extinterp(clustergrp(i
).ind(j)+1).data(:,2),'go'); hold on;

plot(flxinterp(clustergrp(i).ind(j)+1).data(:,1),flxinterp(clustergrp(i
).ind(j)+1).data(:,2),'bo')
    end
    plot(ang_matrix_avg,mov_matrix_avg,'k-','LineWidth',4);
    xlabel('Angle (degrees)','FontSize',20)
    ylabel('Force (N)', 'FontSize',20)
end
```

```
%% Perform the angle-force area calculation

anglecrop = 5/0.1;  % cropping both sides by 5 degrees (sampling rate
0.1 Hz)
for i=1:min(length(ext_new),length(flx_new)),
    ext_new(i).bounds = 1+anglecrop:length(ext_new(i).data(:,1))-
anglecrop;
    flx_new(i).bounds = 1+anglecrop:length(flx_new(i).data(:,1))-
anglecrop;
    area(i) = (sum(ext_new(i).data(ext_new(i).bounds,2))-
sum(flx_new(i).data(flx_new(i).bounds,2)))*0.1;
    area_norm(i) =
area(i)/mean([length(ext_new(i).bounds),length(ext_new(i).bounds)]);
    if area_norm(i)==Inf
        area_norm(i)=NaN;
    end
    if area_norm(i)==-Inf
        area_norm(i)=NaN;
    end
end
area_mean = mean(area);
area_stdev = std(area);
area_norm_mean = nanmean(area_norm);
area_norm_stdev = nanstd(area_norm);
area_export=[area_mean;area_stdev;area_norm_mean;area_norm_stdev];
```